Supporting Information

Chiral biphenanthrene-diol-based lanthanide cubanes

Haowei Qin,[ab] Tingting Wang,[ab] Tingting Feng,[ab] Zhenhua Zhu,[c] Xu Ying,*[c] Peng Zhang*[ab] and Jinkui Tang*[abc]

[a]State Key Laboratory of Rare Earth Resource Utilization, Changchun Institute of Applied Chemistry, Chinese Academy of Sciences, Changchun 130022, P. R. China. Email: pengzhang@ciac.ac.cn
[b]School of Applied Chemistry and Engineering, University of Science and Technology of China, Hefei 230026, P. R. China.
[c]School of Chemistry and Chemical Engineering, Beijing Institute of Technology, Beijing 102488, P. R. China. Email: jtang@bit.edu.cn, xu-ying@bit.edu.cn

Contents

1.Synthesis and characterization

General procedure

Unless otherwise noted, all oxygen- or moisture-sensitive reactions were conducted in flame-dried glassware under an atmosphere of nitrogen (N_2). Commercial reagents were used as received without further purification. Coordination reactions were carried out under ambient air. *R/S*-4,4′-biphenanthrene-3,3′-diol (***R***/***S*-H_2L**) was synthesized according to the previously reported procedure.[1-3] Photochemical irradiations employed a 500W high-pressure mercury lamp.[1] The product was purified by column chromatography using 200-300 mesh silica gel (eluent: petroleum ether/ethyl acetate = 20:1, v/v).

Measurements

^{1}H NMR spectra were recorded on Bruker Avance 400 MHz spectrometer, with chemical shifts referenced to residual solvent peaks ($CDCl_3$: δ 7.26 ppm; CD_3OD: δ 3.31 ppm). Elemental microanalyses (C, H, N) were performed on a Perkin Elmer 2400 analyzer. UV-Vis absorption spectra were performed on UV-1750 UV-Vis spectrophotometer. The solution circular dichroism (CD) spectra were measured at 298 K on a Jasco J-1500 spectropolarimeter using quartz cells of 10 mm light path length. TGA was performed on a PerkinElmer TGA 4000 simultaneous thermal analyzer under a nitrogen atmosphere with a heating rate of 10 K/min from 30 to 800 °C. Magnetic property measurements were conducted using a Quantum Design MPMS-XL7 SQUID magnetometer equipped with a 7 T superconducting magnet. DC magnetic susceptibility data were collected over the temperature range of 2-300 K under an applied field of 600 Oe. Isothermal magnetization measurements were performed at 2 K with magnetic fields up to 7 T. AC susceptibility measurements were carried out using a Quantum Design MPMS3 magnetometer with an oscillating field of 3 Oe. The experimental magnetic susceptibility data were corrected for diamagnetic contributions estimated from Pascal's constants and sample holder calibrations.[4]

Synthesis

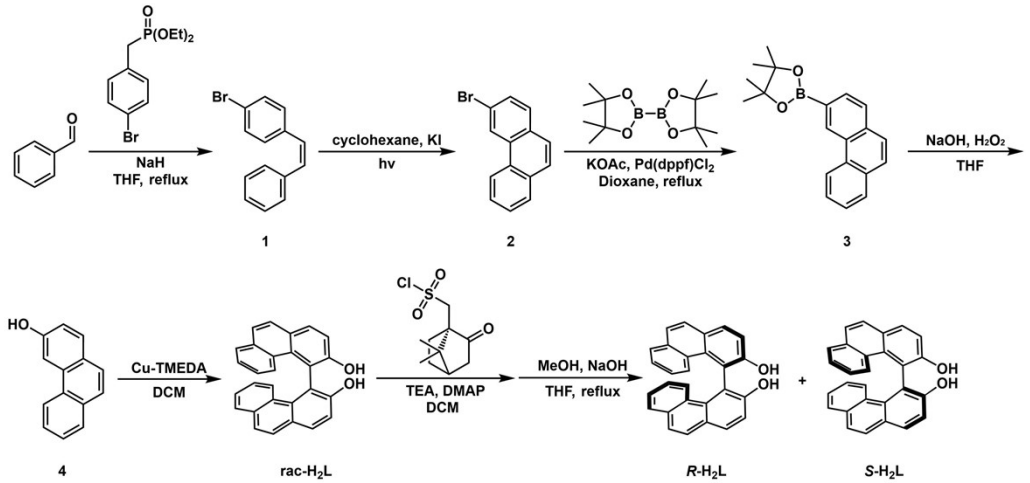

Scheme S1. Synthetic routines of ***R*-H_2L** and ***S*-H_2L**.

Synthesis of (*E*)-1-bromo-4-styrylbenzene (**1**)

Under a nitrogen atmosphere, a dry 500mL round-bottom was charged with dry THF (100 mL) and

cooled in an ice-water bath. With continuous N_2 purging, Sodium hydride (60% in mineral oil, 4.98 g, 124.4 mmol, 1.1 equiv) and diethyl 4-bromobenzylphosphonate (38.20 g, 124.4 mmol, 1.1 equiv) were added sequentially, followed by dropwise addition of a solution of Benzaldehyde (12.00 g, 113.08 mmol, 1 equiv) in anhydrous THF (20 mL). The mixture was stirred at 0 °C for 20 min, then refluxed at 70°C in an oil bath for 24 h. The reaction was quenched with water (250 mL) and filtered. The collected solid was washed sequentially with water and N-pentane, then dried to give product **1** as a white solid (27.70 g, 95% yield). **^{1}H NMR** (400 MHz, $CDCl_3$) δ (ppm): 7.49 (dd, *J* = 10.8, 8.0 Hz, 4H), 7.42-7.33 (m, 4H), 7.29 (d, *J* = 7.3 Hz, 1H), 7.14-7.00 (m, 2H).

Synthesis of 3-bromophenanthrene (**2**)

(*E*)-1-bromo-4-styrylbenzene (**1**) (0.55 g, 2.1 mmol, 1 equiv) and potassium iodide (0.35g, 2.1 mmol, 1 equiv) were charged into a 1 L volumetric flask, followed by the addition of 1 L cyclohexane. The mixture was irradiated with a Hg lamp (500 W) for 9 h. Then, the solvent was removed by rotary evaporation under reduced pressure. The resulting residue was taken up in dichloromethane, and the solution was washed sequentially with sodium bisulfite solution and saturated brine. The organic phase was dried over anhydrous Na_2SO_4, filtered, and the solvent was again removed via rotary evaporation under reduced pressure to yield the crude product. Purification of the crude material by silica gel column chromatography (eluent: petroleum ether) afforded the target product **2** (0.27 g, 1.1 mmol, 50% yield) as a white solid. **^{1}H NMR** (400 MHz, $CDCl_3$) δ (ppm): 8.82 (s, 1H), 8.60 (d, *J* = 8.1 Hz, 1H), 7.89 (d, *J* = 7.8 Hz, 1H), 7.76 (d, *J* = 8.6 Hz, 2H), 7.73-7.59 (m, 4H).

Synthesis of 4,4,5,5-tetramethyl-2-(phenanthren-3-yl)-1,3,2-dioxaborolane (**3**)

A 500 mL flame-dried round-bottom flask was charged with anhydrous 1,4-dioxane (100 mL) under nitrogen atmosphere. To this solution were sequentially added 3-bromophenanthrene (**2**) (8.42 g, 32.7 mmol, 1 equiv), 4,4,4′,4′,5,5,5′,5′-octamethyl-2,2'-bi(1,3,2-dioxaborolane) (9.98 g, 39.3 mmol, 1.2 equiv), potassium acetate (12.21 g, 124.4 mmol, 3.8 equiv), and 1,1′-ferrocenediyl-bis (diphenylphosphine) (0.96 g, 1.3 mmol, 4%). The reaction mixture refluxed at 100 °C in an oil bath for 18 h. The reaction mixture was filtered, and the filtrate was dried over anhydrous magnesium sulfate. The solvent was then removed by rotary evaporation. Purification of the crude material by silica gel column chromatography (eluent: petroleum ether/ethyl acetate = 20:1, v/v) afforded the target product **3** (6.97g, 22.9 mmol, 70% yield) as a white solid. **^{1}H NMR** (400 MHz, $CDCl_3$) δ (ppm): 9.20 (s, 1H), 8.85 (d, *J* = 8.2 Hz, 1H), 8.00 (d, *J* = 7.9 Hz, 1H), 7.88 (dd, *J* = 7.9, 2.9 Hz, 2H), 7.81-7.71 (m, 2H), 7.67 (t, *J* = 1.3 Hz, 1H), 7.63-7.57 (m, 1H), 1.42 (s, 12H).

Synthesis of phenanthren-3-ol (**4**)

In a 500 mL glass flask, THF (200 mL) and 4,4,5,5-tetramethyl-2-(phenanthren-3-yl)- 1,3,2-dioxaborolane (**3**) (7.47 g, 24.6 mmol, 1 equiv) were added sequentially. The mixture was cooled to 0 °C in an ice-water bath. While maintaining this temperature, sodium hydroxide (5.89 g, 147.3 mmol, 6 equiv) was added, followed by dropwise addition of hydrogen peroxide solution (15.05 mL, 30%, 147.3 mmol, 6 equiv). The reaction mixture was stirred at this temperature for 2 h. Upon completion, the reaction was quenched with saturated ammonium chloride solution (100 mL). The mixture was extracted with ethyl acetate (3 × 50 mL), and the organic phases were combined. The organic layer was washed sequentially with deionized water (50 mL) and saturated sodium chloride solution (50 mL), then dried over anhydrous sodium sulfate. After filtration, the filtrate was concentrated by rotary

evaporation. The crude product was purified by silica gel column chromatography (eluent: petroleum ether/ethyl acetate = 20:1, v/v) to afford phenanthren-3-ol (**4**) (4.29 g, 90% yield) as a white solid. **^{1}H NMR** (400 MHz, CD_3OD) δ (ppm): 7.49 (d, J = 7.5 Hz, 2H), 7.39 (d, *J* = 8.5 Hz, 2H), 7.31 (t, *J* = 7.6 Hz, 2H), 7.19 (t, *J* = 7.4 Hz, 1H), 7.08 (d, *J* = 16.4 Hz, 1H), 6.96 (d, *J* = 16.4 Hz, 1H), 6.77 (d, *J* = 8.6 Hz, 2H).

Synthesis of 4,4'-biphenanthrene-3,3'-diol (**rac-H_2L**)

Under a nitrogen atmosphere, a dry 250 mL round-bottom was charged with dry DCM (60 mL). With continuous N_2 purging, phenanthren-3-ol (2.00 g, 10.3 mmol, 1.0 equiv) and Cu-TMEDA (0.96 g, 2.1 mmol, 0.2 equiv) were added sequentially. The reaction mixture was stirred at 25 ℃ for 12 h, then quenched with saturated ammonium chloride solution (100 mL). The resulting mixture was separated, and the organic layer was dried over anhydrous sodium sulfate. After solvent removal by rotary evaporation, the crude product was purified by silica gel column chromatography (eluent: petroleum ether/ethyl acetate = 20:1, v/v) to afford the target product **rac-H_2L** (0.80 g, 2.1 mmol, 40% yield) as a white solid. **^{1}H NMR** (400 MHz, $CDCl_3$) δ (ppm): 8.11-8.06 (m, 2H), 8.06-8.00 (m, 2H), 7.87-7.81 (m, 4H), 7.73 (d, *J* = 8.8 Hz, 2H), 7.45 (d, *J* = 8.6 Hz, 2H), 7.39 (t, *J* = 7.4 Hz, 2H), 6.95 (ddd, *J* = 8.6, 7.0, 1.4 Hz, 2H), 5.01 (s, 2H).

Synthesis of *P*/*M*-4,4′-Biphenanthrene-3,3′-dicamphorsulfonicester

A 500 mL flame-dried round-bottom flask, maintained under nitrogen atmosphere, was charged with dry DCM (100 mL) and cooled in an ice-water bath. To this cooled solution were sequentially added 4,4′-biphenanthrene-3,3′-diol (**rac-H_2L**) (3.64 g, 9.4 mmol, 1 equiv), triethylamine (5.89 mL, 42.4 mmol, 4.5 equiv), and 4-dimethylaminopyridine (DMAP) (0.69 g, 5.7 mmol, 0.6 equiv). (1S)-(+)-10-Camphorsulfonyl chloride (8.29 g, 32.3 mmol, 3.5 equiv) was dissolved in anhydrous dichloromethane (40 mL) and added dropwise to the reaction mixture at 0 °C. The reaction was then stirred at 0 °C for 20 min and subsequently at room temperature for 18 h. The reaction was quenched with water (150 mL) and the organic phase was separated via liquid-liquid extraction. The organic phase were dried over anhydrous Na_2SO_4, filtered, and concentrated using a rotary evaporator under reduced pressure. The crude product was purified by silica gel column chromatography (eluent: dichloromethane/ethyl acetate = 200:1, v/v) to afford two diastereomers. (3.34 g, 64% yield) (***P***: 2.11 g, ***M***: 1.23 g)

Synthesis of *S*-4,4′-biphenanthrene-3,3′-diol (***S*-H_2L**)

A 250 mL round-bottom flask was charged with tetrahydrofuran (60 mL). To this solution were sequentially added compound *P*-4,4′-Biphenanthrene-3,3′- dicamphorsulfonicester (2.64 g, 4.7 mmol), methanol (26.4 mL), and sodium hydroxide (5 M, 26.4 mL). The reaction mixture refluxed at 90 °C in an oil bath for 15 h. After cooling to room temperature, 1 M hydrochloric acid was added to the reaction mixture until it was acidic (pH 3-4). The methanol was removed under reduced pressure, and the product extracted with DCM. Then the combined organic layers were dried over anhydrous Na_2SO_4. Following filtration, the solvent was evaporated under reduced pressure to afford the crude product. The crude product was purified by silica gel column chromatography (eluent: petroleum ether/ethyl acetate = 20:1, v/v) to afford the target product ***S*-H_2L** as a white solid (1.28 g, 3.3 mmol, 70% yield). **^{1}H NMR** (400 MHz, $CDCl_3$) δ (ppm): 8.09 (d, *J* = 8.7 Hz, 2H), 8.03 (d, *J* = 8.7 Hz, 2H), 7.88-7.80 (m, 4H), 7.74 (d, *J* = 8.8 Hz, 2H), 7.45 (d, *J* = 8.6 Hz, 2H), 7.42-7.36 (m, 2H), 6.95 (ddd, *J* = 8.6, 7.0, 1.4 Hz, 2H), 5.02 (s, 2H).

Synthesis of *R*-4,4′-biphenanthrene-3,3′-diol (***R*-H_2L**)

The synthetic procedure of ***R*-H_2L** is similar to ***S*-H_2L**, except that ***M*-**4,4′-Biphenanthrene-3,3′-dicamphorsulfonicester was used rather than ***P*-**4,4′-Biphenanthrene-3,3′-dicamphorsulfonicester. (1.44 g, 3.7 mmol, 72% yield) **^{1}H NMR** (400 MHz, $CDCl_3$) δ (ppm): 8.09 (d, *J* = 8.7 Hz, 2H), 8.03 (d, *J* = 8.7 Hz, 2H), 7.90 – 7.79 (m, 4H), 7.74 (d, *J* = 8.8 Hz, 2H), 7.45 (d, *J* = 8.6 Hz, 2H), 7.42-7.36 (m, 2H), 6.98-6.91 (m, 2H), 5.01 (s, 2H).

Synthesis of ***R*-Dy_4**

R-4,4′-biphenanthrene-3,3′-diol (***R*-H_2L**) (23.19 mg, 0.06 mmol) was dissolved in DCM (10 mL). After stirring for 2 minutes, 1,1,3,3-Tetramethylguanidine (TMG) (15 μL, 0.12 mmol) was introduced and the mixture was stirred for an additional 10 minutes. A methanolic solution (1.5 mL) of $Dy(NO_3)_3{\cdot}5H_2O$ (8.77 mg, 0.02 mmol) was then added dropwise, followed by continuous stirring at 25 °C for 20 minutes. The resulting mixture was filtered through a medium-porosity filter paper and transferred to a 20 mL glass vial. Crystallization was achieved through slow vapor diffusion of n-pentane (10 mL) into the dichloromethane solution over 10 days at 25 °C, yielding X-ray quality yellow crystals (6.5 mg, 32% yield based on Dy). Elemental analysis (%) calcd for $C_{195}H_{173}Cl_{14}Dy_4N_{12}O_{17.5}$ (M_W = 4110.74): C, 64.62; H, 4.64; N, 4.81. Found: C, 62.32; H, 4.46; N, 4.79. FTIR ν/cm^{-1} (ATR): 548.99 (m), 642.22 (s), 708.82 (s), 748.18 (s), 795.62 (s), 834.82(s), 864.16 (w), 920.03 (s), 1034.36 (m), 1087.52 (m), 1100.89 (m), 1132.97 (m), 1160.54 (m), 1215.47(m), 1269.64 (s), 1309.96 (s), 1404.61 (m), 1411.82 (m), 1496.05 (s), 1581.22 (m), 1647.21 (w), 3033.18 (w), 3564.2 (w).

Synthesis of ***S*-Dy_4**

The synthetic procedure of ***S*-Dy_4** is similar to ***R*-Dy_4**, except that *S*-4,4′-biphenanthrene-3,3′-diol (***S*-H_2L**) was used rather than *R*-4,4′-biphenanthrene-3,3′-diol (***R*-H_2L**). (6.5 mg, 32% yield based on Dy). Elemental analysis (%) calcd for $C_{195}H_{173}Cl_{14}Dy_4N_{12}O_{17.5}$ (M_W = 4110.74): C, 64.60; H, 4.67; N, 4.81. Found: C, 64.10; H, 4.14; N, 4.99. FTIR ν/cm^{-1} (ATR): 528.21 (s), 555.35 (m), 641.71 (s), 708.7 (s), 747.87 (s), 795.39 (s), 834.67 (s), 864.14 (m), 919.94 (s), 1034.3 (m), 1087.33 (m), 1100.77 (m), 1137.55(m), 1215.32 (m), 1269.48 (s), 1309.33 (s), 1404.25 (m), 1411.79 (w), 1581.15 (m), 1646.45 (w), 3033.45 (w), 3563.82 (w).

Synthesis of ***R*-Er_4**

R-4,4′-biphenanthrene-3,3′-diol (***R*-H_2L**) (23.19 mg, 0.06 mmol) was dissolved in DCM (10 mL). After stirring for 2 minutes, 1,1,3,3-Tetramethylguanidine (TMG) (15 μL, 0.12 mmol) was introduced and the mixture was stirred for an additional 10 minutes. A methanolic solution (1.5 mL) of $Er(NO_3)_3{\cdot}5H_2O$ (8.87 mg, 0.02 mmol) was then added dropwise, followed by continuous stirring at 25 °C for 20 minutes. The resulting mixture was filtered through a medium-porosity filter paper and transferred to a 20 mL glass vial. Crystallization was achieved through slow vapor diffusion of n-pentane (10 mL) into the dichloromethane solution over 7 days at 25 °C, yielding X-ray quality yellow crystals (6.5 mg, 32% yield based on Er). Elemental analysis (%) calcd for $C_{195}H_{172}Cl_{14}Er_4N_{12}O_{17}$ (M_W = 4120.78): C, 64.16; H, 4.74; N, 4.78. Found: C, 63.57; H, 4.47; N, 4.86. FTIR ν/cm^{-1} (ATR): 529 (m), 555.44 (m), 628.34 (s), 651.07 (s), 709.15 (s), 748.43 (s), 796.21 (s), 835.38 (s), 864.31 (w), 920.45 (s), 1034.77 (m), 1087.57 (m), 1101.01 (m), 1132.95 (m), 1160.43 (w), 1215.54 (m), 1270.1 (s), 1310.62 (s), 1404.85 (m), 1441.92 (s), 1496.12 (s), 1581.32 (m), 1645.77 (w), 3030.55 (w),

3565.02 (w).

Synthesis of ***S*-Er$_4$**

The synthetic procedure of ***S*-Er$_4$** is similar to ***R*-Er$_4$**, except that *S*-4,4′-biphenanthrene-3,3′-diol (***S*-H$_2$L**) was used rather than *R*-4,4′-biphenanthrene-3,3′diol (***R*-H$_2$L**). (6.5 mg, 32% yield based on Er). Elemental analysis (%) calcd for $C_{194}H_{171}Cl_{14}Er_4N_{12}O_{17.5}$ (M_W = 4044.86): C, 64.40; H, 4.74; N, 4.75. Found: C, 63.57; H, 4.52; N, 4.85. FTIR ν/cm^{-1} (ATR): 532.91 (m), 556.6 (m), 575.11 (m), 628.56 (s), 651.36 (s), 709.43 (s), 748.69 (s), 796.09 (s), 836.29 (s), 864.18 (w), 920.7 (s), 1034.77 (m), 1087.79 (m), 1101.09 (m), 1138.81 (m), 1160.37 (w), 1215.5 (m), 1270.51 (s), 1311.33 (s), 1404.81 (m), 1442.21 (s), 1496.23 (m), 1581.46 (m), 1646.46 (w), 3033.33 (w), 3564.83 (w).

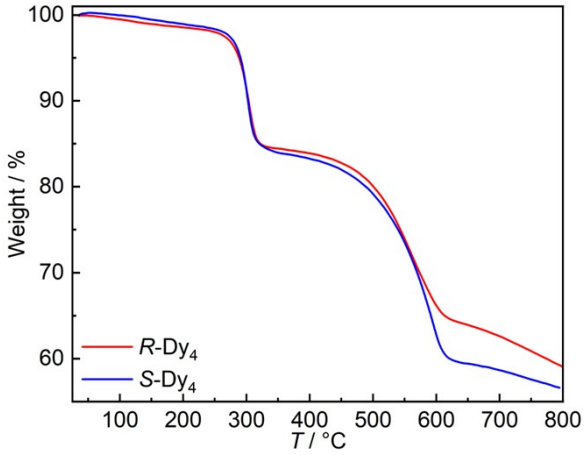

Figure S1. TGA curves of ***R*-Dy$_4$** (red line) and ***S*-Dy$_4$** (blue line).

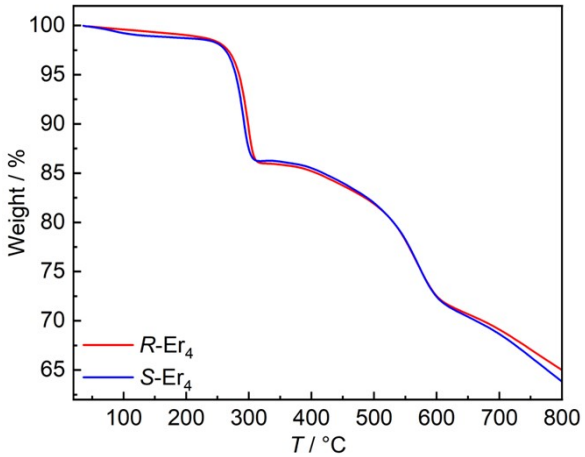

Figure S2. TGA curves of ***R*-Er$_4$** (red line) and ***S*-Er$_4$** (blue line).

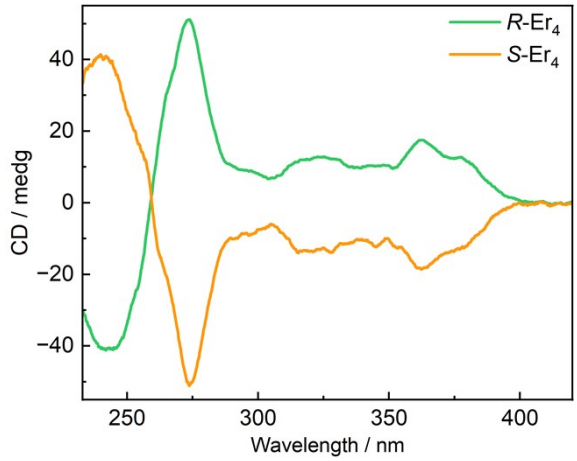

Figure S3. Circular dichroism (CD) spectra of ***R*/*S*-Er$_4$** (2.50×10^{-6} M) in DCM.

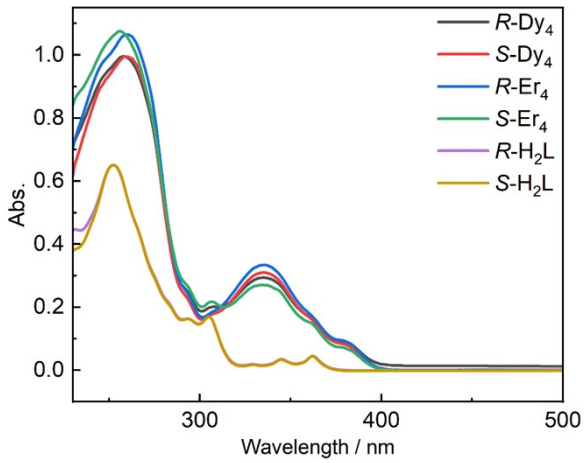

Figure S4. UV-vis absorption spectra of ***R*/*S*-Dy$_4$** ($c = 2.50 \times 10^{-6}$ M), ***R*/*S*-Er$_4$** ($c = 2.50 \times 10^{-6}$ M) and ***R*/*S*-H$_2$L** ($c = 1.00 \times 10^{-5}$ M) in DCM.

NMR spectra

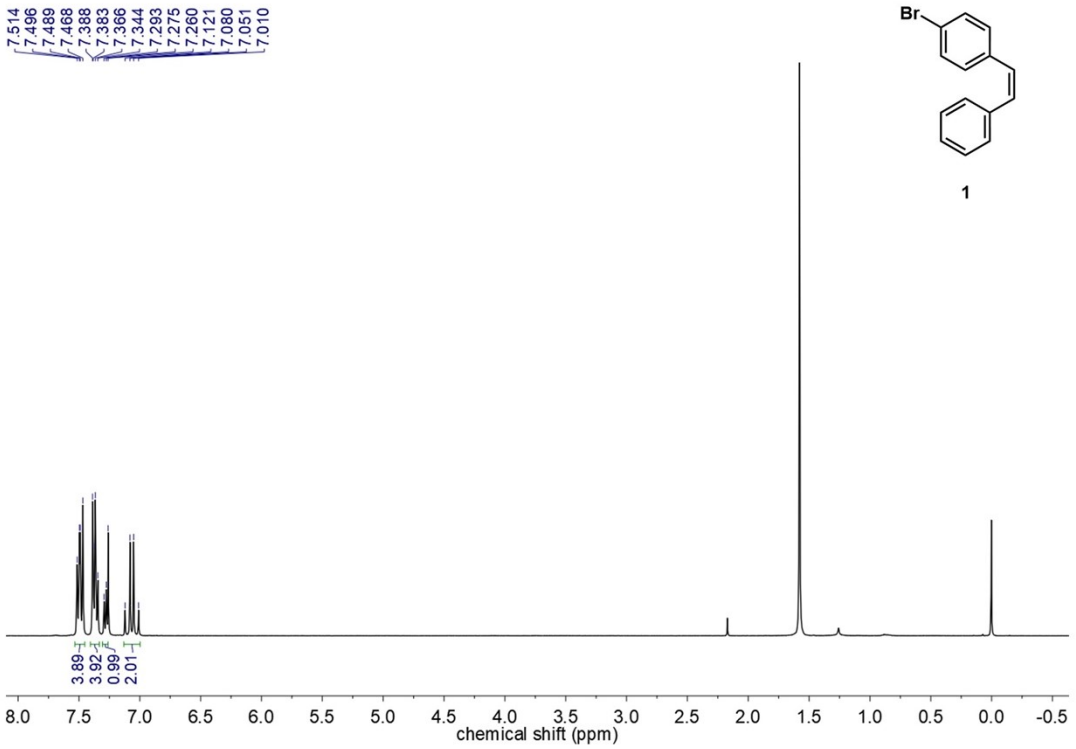

Figure S5. ^{1}H-NMR (400 MHz) spectrum of **1** in $CDCl_3$.

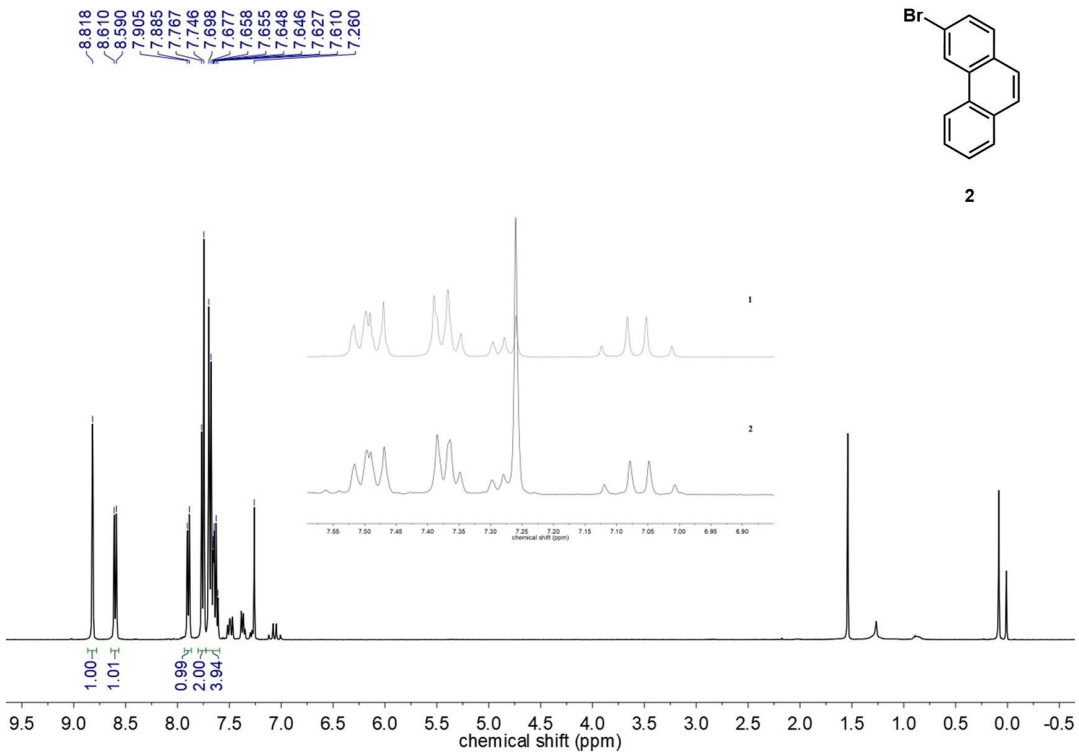

Figure S6. ^{1}H-NMR (400 MHz) spectrum of **2** in $CDCl_3$. The signals in 6.95-7.55 ppm are assigned to the compound **1**.

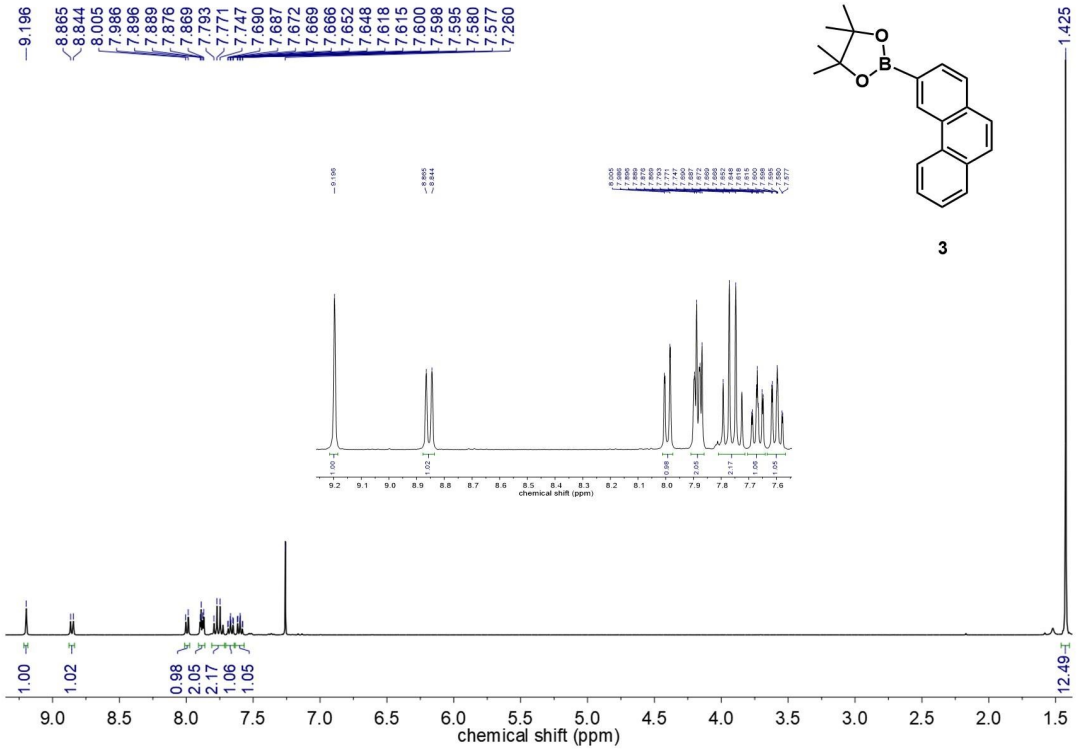

Figure S7. ^{1}H-NMR (400 MHz) spectrum of **3** in $CDCl_3$.

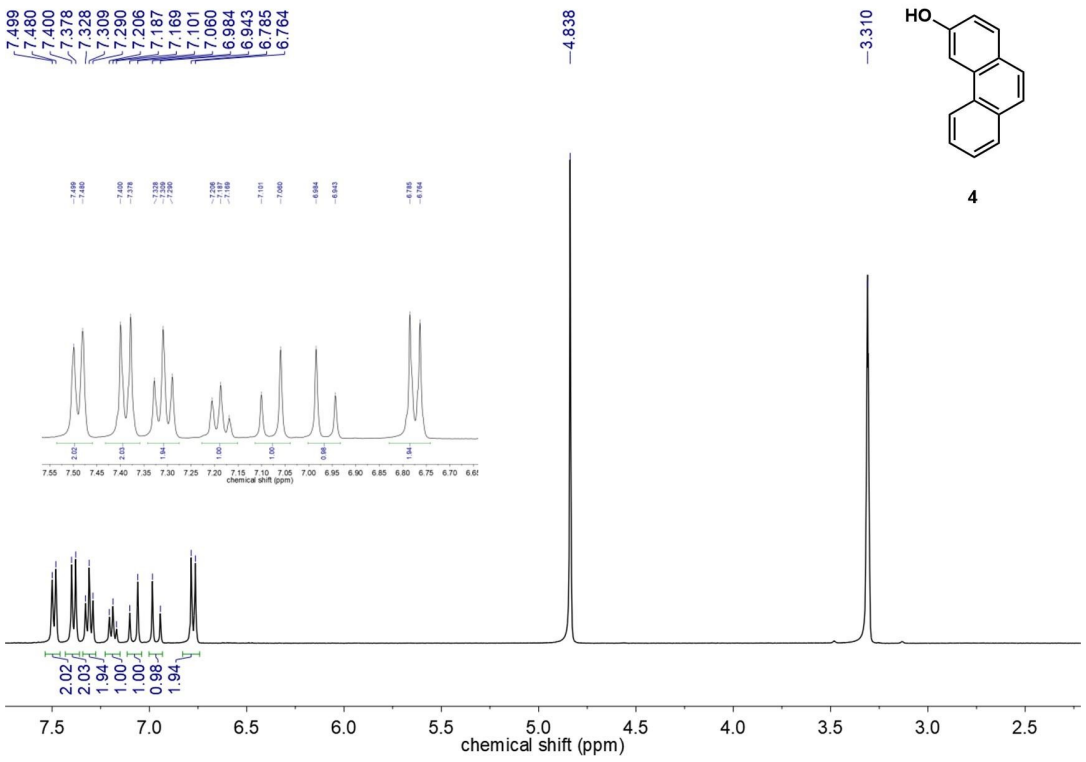

Figure S8. ^{1}H-NMR (400 MHz) spectrum of **4** in DMSO.

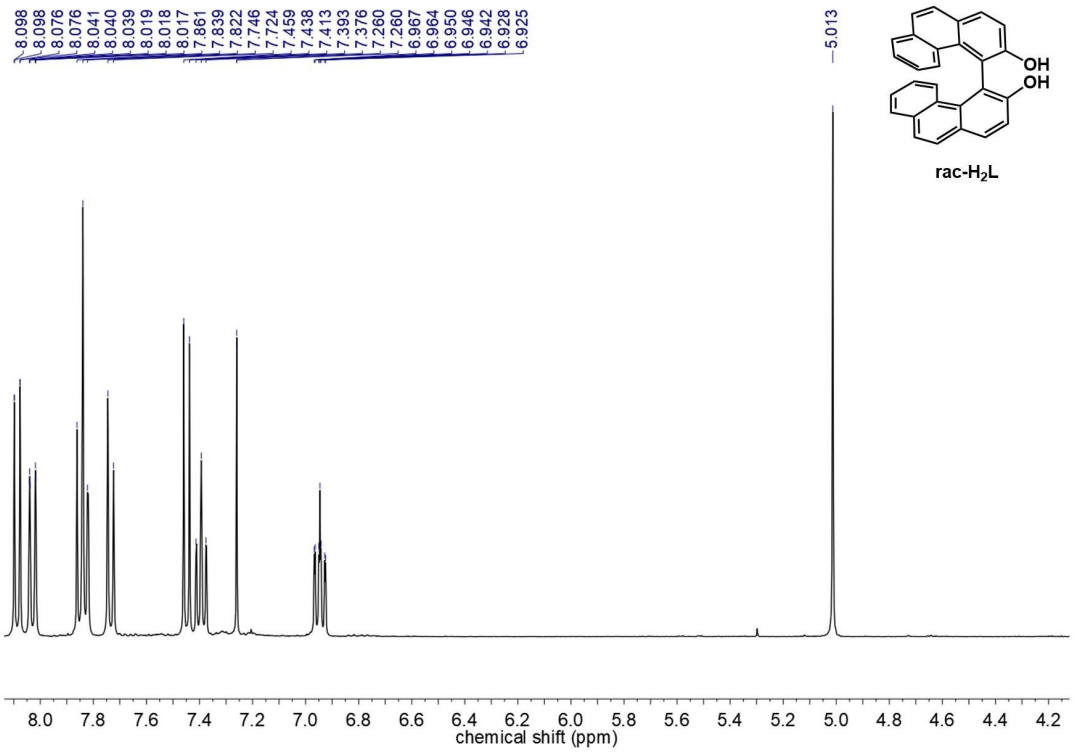

Figure S9. ^{1}H-NMR (400 MHz) spectrum of **rac-H_2L** in $CDCl_3$.

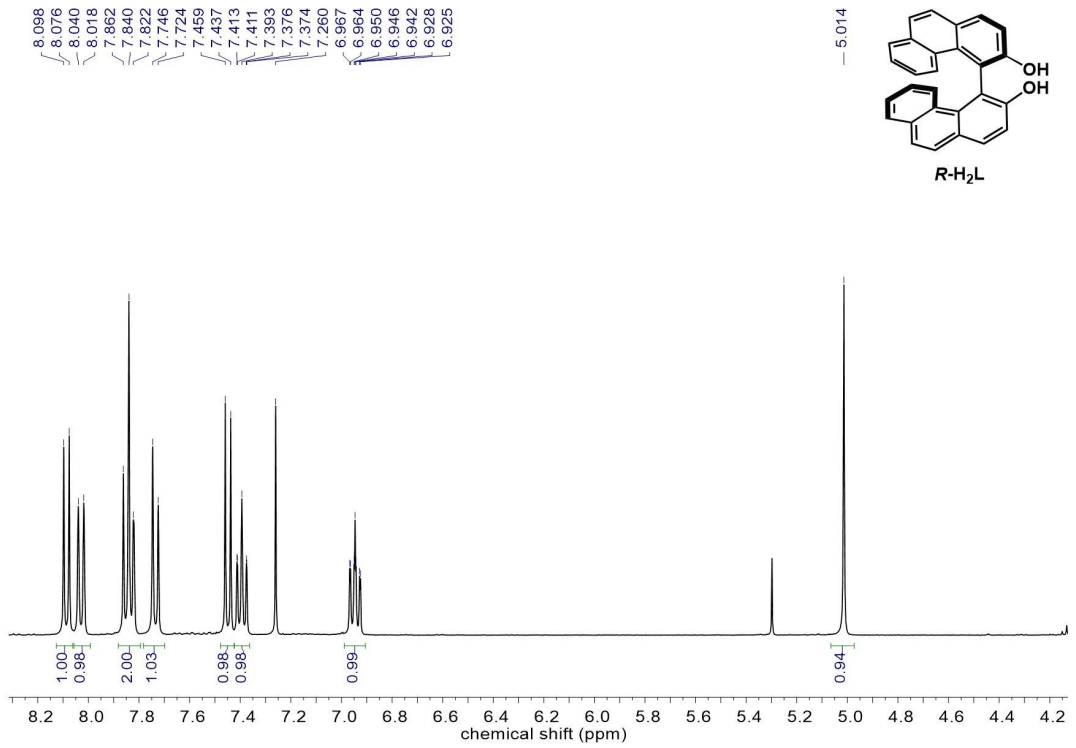

Figure S10. ^{1}H-NMR (400 MHz) spectrum of ***R*-H_2L** in $CDCl_3$.

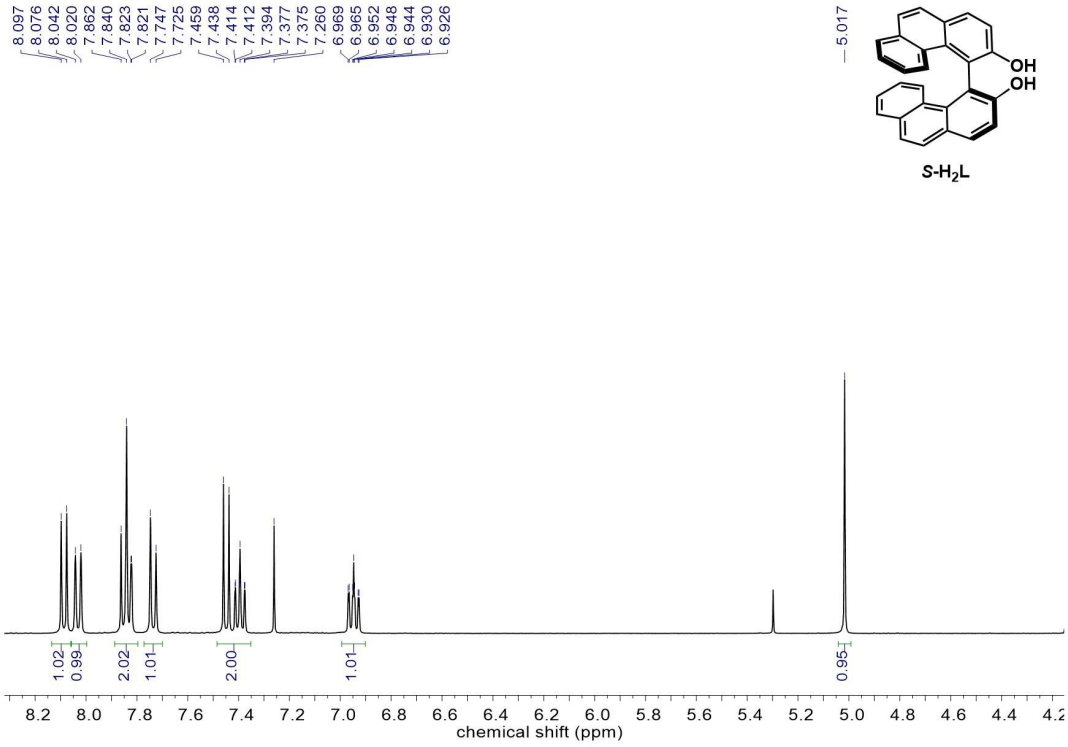

Figure S11. ^{1}H-NMR (400 MHz) spectrum of ***S*-H_2L** in $CDCl_3$.

2. X-ray crystallography

Single-crystal X-ray data for ***R*-Dy$_4$**, ***S*-Dy$_4$**, ***R*-Er$_4$** and ***S*-Er$_4$** were recorded on a Bruker SMART APEX diffractometer equipped with graphite-monochromatized MoKα radiation (λ = 0.71073 Å) at 180 K. The structures were solved in Olex2 with SHELXT using intrinsic phasing and were refined with SHELXL using least squares minimization.[5-7] All non-hydrogen atoms were refined anisotropically. All hydrogen atom positions were calculated geometrically and refined using the riding model. Crystallographic data, refinement details are given in Tables S1 - S8.

Table S1. Crystal data and structure refinement for ***R*-Dy$_4$** and ***S*-Dy$_4$**.

Compound reference	***R*-Dy$_4$**	***S*-Dy$_4$**
Chemical formula	$C_{195}H_{173}Cl_{14}Dy_4N_{12}O_{17.5}$	$C_{195}H_{173}Cl_{14}Dy_4N_{12}O_{17.5}$
Formula Mass	4110.74	4110.74
Crystal system	orthorhombic	orthorhombic
a (Å)	17.5839(7)	17.7008(6)
b (Å)	28.4582(14)	28.3765(12)
c (Å)	35.8538(16)	36.0385(15)
α (°)	90	90
β (°)	90	90
γ (°)	90	90
Unit cell volume (Å^3)	17941.5(14)	18101.7(12)
Temperature (K)	180.0	180.0
Space group	$P2_12_12_1$	$P2_12_12_1$
Z	4	4
ρ_{calc} (g/cm^3)	1.522	1.508
F (000)	8276	8276.0
Radiation	MoKα (λ = 0.71073)	MoKα (λ = 0.71073)
Reflections collected	99399	100598
Independent reflections	31698	31806
R_{int}	0.1437	0.1205
GOF on F^2	1.013	1.029
R_1 (I ≥2 σ (*I*))	0.0694	0.0611
wR_2 (all data)	0.1633	0.1421
Flack parameter	0.023(7)	0.008(6)
CCDC number	2520050	2520049

Table S2. Selected bond distances (Å) for ***R*-Dy$_4$** and ***S*-Dy$_4$**.

***R*-Dy$_4$**	***S*-Dy$_4$**
Dy1-O1 2.3793(9)	Dy1-O1 2.3792(8)
Dy1-O2 2.3863(9)	Dy1-O2 2.3660(7)
Dy1-O3 2.3691(9)	Dy1-O3 2.3892(7)
Dy1-O5 2.185(13)	Dy1-O5 2.153(12)
Dy1-O6 2.146(12)	Dy1-O6 2.161(11)
Dy1-O7 2.118(14)	Dy1-O7 2.180(10)
Dy2-O1 2.4126(8)	Dy2-O1 2.3945(7)

Dy2-O2 2.3797(8)	Dy2-O3 2.3952(7)
Dy2-O4 2.3792(8)	Dy2-O4 2.3955(7)
Dy2-O8 2.236(12)	Dy2-O8 2.171(10)
Dy2-O9 2.139(12)	Dy2-O9 2.175(11)
Dy2-O10 2.159(12)	Dy2-O10 2.227(10)
Dy3-O2 2.3881(8)	Dy3-O2 2.3638(7)
Dy3-O3 2.3841(8)	Dy3-O3 2.3948(7)
Dy3-O4 2.4133(8)	Dy3-O4 2.3984(7)
Dy3-O11 2.164(12)	Dy3-O11 2.156(10)
Dy3-O12 2.212(12)	Dy3-O12 2.203(10)
Dy3-O13 2.189(12)	Dy3-O13 2.174(10)
Dy4-O1 2.3859(8)	Dy4-O1 2.3944(7)
Dy4-O3 2.3934(9)	Dy4-O2 2.3689(7)
Dy4-O4 2.4025(8)	Dy4-O4 2.4125(7)
Dy4-O14 2.132(12)	Dy4-O14 2.122(10)
Dy4-O15 2.130(12)	Dy4-O15 2.107(9)
Dy4-O16 2.183(11)	Dy4-O16 2.202(10)

Table S3. Selected bond angles (°) for ***R*-Dy$_4$** and ***S*-Dy$_4$**.

***R*-Dy$_4$**	***S*-Dy$_4$**
O1-Dy1-O2 73.90(3)	O1-Dy1-O3 73.98(2)
O3-Dy1-O1 74.38(3)	O2-Dy1-O1 73.61(2)
O3-Dy1-O2 73.96(3)	O2-Dy1-O3 73.50(2)
O5-Dy1-O1 87.7(4)	O5-Dy1-O1 159.7(3)
O5-Dy1-O2 100.8(3)	O5-Dy1-O2 96.7(3)
O5-Dy1-O3 162.1(4)	O5-Dy1-O3 86.3(3)
O6-Dy1-O1 97.1(4)	O5-Dy1-O6 99.4(4)
O6-Dy1-O2 161.5(4)	O5-Dy1-O7 101.1(4)
O6-Dy1-O3 88.2(3)	O6-Dy1-O1 98.0(3)
O6-Dy1-O5 94.8(4)	O6-Dy1-O2 87.7(3)
O7-Dy1-O1 159.4(3)	O6-Dy1-O3 161.0(3)
O7-Dy1-O2 86.2(3)	O6-Dy1-O7 96.4(4)
O7-Dy1-O3 95.3(3)	O7-Dy1-O1 87.3(3)
O7-Dy1-O5 101.5(5)	O7-Dy1-O2 160.8(3)
O7-Dy1-O6 100.4(5)	O-Dy1-O3 100.4(3)
O2-Dy2-O1 73.41(2)	O1-Dy2-O3 73.59(2)
O4-Dy2-O1 72.82(2)	O1-Dy2-O4 72.98(2)
O4-Dy2-O2 73.57(2)	O3-Dy2-O4 73.53(2)
O8-Dy2-O1 89.0(3)	O8-Dy2-O1 163.2(3)
O8-Dy2-O2 162.1(3)	O8-Dy2-O3 100.2(3)
O8-Dy2-O4 98.3(3)	O8-Dy2-O4 90.3(3)
O9-Dy2-O1 97.5(3)	O8-Dy2-O9 97.5(4)
O9-Dy2-O2 87.6(3)	O8-Dy2-O10 95.6(4)
O9-Dy2-O4 160.5(4)	O9-Dy2-O1 97.8(3)

O9-Dy2-O8 98.3(5)	O9-Dy2-O3 87.6(3)
O9-Dy2-O10 98.0(5)	O9-Dy2-O4 160.6(3)
O10-Dy2-O1 162.5(3)	O9-Dy2-O10 97.8(4)
O10-Dy2-O2 99.1(3)	O10-Dy2-O1 89.1(3)
O10-Dy2-O4 90.0(3)	O10-Dy2-O3 162.5(3)
O10-Dy2-O8 96.8(5)	O10-Dy2-O4 99.1(3)
O2-Dy3-O4 72.81(2)	O2-Dy3-O3 73.44(2)
O3-Dy3-O2 73.65(2)	O2-Dy3-O4 74.03(2)
O3-Dy3-O4 75.02(2)	O3-Dy3-O4 73.488(19)
O11-Dy3-O2 86.2(3)	O11-Dy3-O2 101.2(2)
O11-Dy3-O3 159.7(3)	O11-Dy3-O3 160.0(3)
O11-Dy3-O4 101.8(3)	O11-Dy3-O4 86.6(3)
O11-Dy3-O12 95.0(5)	O11-Dy3-O12 101.7(4)
O11-Dy3-O13 99.4(4)	O11-Dy3-O13 98.2(4)
O12-Dy3-O2 97.7(3)	O12-Dy3-O2 86.2(3)
O12-Dy3-O3 85.4(3)	O12-Dy3-O3 97.1(3)
O12-Dy3-O4 159.9(3)	O12-Dy3-O4 159.8(3)
O13-Dy3-O2 158.6(3)	O13-Dy3-O2 159.6(3)
O13-Dy3-O3 100.3(3)	O13-Dy3-O3 86.1(3)
O13-Dy3-O4 85.8(3)	O13-Dy3-O4 100.8(3)
O13-Dy3-O12 102.3(4)	O13-Dy3-O12 96.3(4)
O1-Dy4-O3 73.82(2)	O1-Dy4-O4 72.69(2)
O1-Dy4-O4 72.88(2)	O2-Dy4-O1 73.28(2)
O3-Dy4-O4 75.05(2)	O2-Dy4-O4 73.68(2)
O14-Dy4-O1 156.9(3)	O14-Dy4-O1 89.1(3)
O14-Dy4-O3 83.4(3)	O14-Dy4-O2 99.9(3)
O14-Dy4-O4 97.8(3)	O14-Dy4-O4 161.7(3)
O14-Dy4-O16 101.4(4)	O14-Dy4-O16 96.1(4)
O15-Dy4-O1 88.3(3)	O15-Dy4-O1 156.4(3)
O15-Dy4-O3 98.7(4)	O15-Dy4-O2 83.6(3)
O15-Dy4-O4 161.1(3)	O15-Dy4-O4 96.6(3)
O15-Dy4-O14 99.2(4)	O15-Dy4-O14 99.7(4)
O15-Dy4-O16 96.5(5)	O15-Dy4-O16 101.3(4)
O16-Dy4-O1 99.4(3)	O16-Dy4-O1 99.4(3)
O16-Dy4-O3 163.1(3)	O16-Dy4-O2 162.2(3)
O16-Dy4-O4 88.2(3)	O16-Dy4-O4 88.7(3)

Table S4. The CShM values calculated by SHAPE 2.1 for ***R*-Dy$_4$** and ***S*-Dy$_4$**.[8, 9]

Central atom	Coordination Geometry	***R*-Dy$_4$**	***S*-Dy$_4$**
Dy1	Octagon (D_{6h})	31.766	31.934
	Pentagonal pyramid (C_{5v})	25.786	24.765
	Octahedron (O_h)	1.315	1.664
	Trigonal prism (D_{3h})	11.760	10.554
	Johnson pentagonal pyramid J2 (C_{5v})	28.947	27.936

Central atom	Coordination Geometry	***R*-Dy$_4$**	***S*-Dy$_4$**
Dy2	Octagon (D_{6h})	32.117	31.806
	Pentagonal pyramid (C_{5v})	24.501	25.351
	Octahedron (O_h)	1.769	1.525
	Trigonal prism (D_{3h})	10.358	11.280
	Johnson pentagonal pyramid J2 (C_{5v})	27.623	28.666

Central atom	Coordination Geometry	***R*-Dy$_4$**	***S*-Dy$_4$**
Dy3	Octagon (D_{6h})	31.962	31.831
	Pentagonal pyramid (C_{5v})	25.376	26.228
	Octahedron (O_h)	1.480	1.368
	Trigonal prism (D_{3h})	11.103	11.508
	Johnson pentagonal pyramid J2 (C_{5v})	28.649	29.484

Central atom	Coordination Geometry	***R*-Dy$_4$**	***S*-Dy$_4$**
Dy4	Octagon (D_{6h})	31.970	32.090
	Pentagonal pyramid (C_{5v})	26.392	25.709
	Octahedron (O_h)	1.316	1.423
	Trigonal prism (D_{3h})	11.826	11.393
	Johnson pentagonal pyramid J2 (C_{5v})	29.577	28.836

Table S5. Crystal data and structure refinement for ***R*-Er$_4$** and ***S*-Er$_4$**.

Compound reference	***R*-Er$_4$**	***S*-Er$_4$**
Chemical formula	$C_{195}H_{172}Cl_{14}Er_4N_{12}O_{17}$	$C_{194}H_{171}Cl_{14}Dy_4N_{12}O_{17.5}$
Formula Mass	4120.78	4044.86
Crystal system	orthorhombic	orthorhombic
a (Å)	17.5439(6)	17.4169(4)
b (Å)	28.4744(11)	28.5045(8)
c (Å)	35.6072(14)	35.6754(11)
α (°)	90	90
β (°)	90	90
γ (°)	90	90
Unit cell volume (Å^3)	17787.6(12)	17711.4(8)
Temperature (K)	180.0	180.0
Space group	$P2_12_12_1$	$P2_12_12_1$
Z	4	4
ρ_{calc} (g/cm^3)	1.539	1.517
F (000)	8288.0	8140.0
Radiation	MoKα (λ = 0.71073)	MoKα (λ = 0.71073)
Reflections collected	100808	100616
Independent reflections	31373	31294
R_{int}	0.0846	0.0663
GOF on F^2	1.016	1.066
R_1 (I ≥2 σ (*I*))	0.0528	0.0562
wR_2 (all data)	0.1305	0.1558
Flack parameter	0.023(5)	0.027(5)
CCDC number	2520051	2520052

Table S6. Selected bond distances (Å) for ***R*-Er$_4$** and ***S*-Er$_4$**.

***R*-Er$_4$**	***S*-Er$_4$**
Er1-O1 2.3697(6)	Er1-O1 2.3582(7)
Er1-O2 2.3536(6)	Er1-O2 2.3323(6)
Er1-O3 2.3379(6)	Er1-O3 2.3525(8)
Er1-O5 2.143(9)	Er1-O5 2.144(12)
Er1-O6 2.147(9)	Er1-O6 2.131(11)
Er1-O7 2.182(10)	Er1-O7 2.164(10)
Er2-O2 2.3708(6)	Er2-O1 2.3674(6)
Er2-O3 2.3532(6)	Er2-O2 2.3424(7)
Er2-O4 2.3861(7)	Er2-O4 2.3647(7)
Er2-O8 2.120(10)	Er2-O8 2.147(10)
Er2-O9 2.120(11)	Er2-O9 2.129(10)
Er2-O10 2.159(9)	Er2-O10 2.189(11)
Er3-O1 2.3699(6)	Er3-O1 2.3680(7)
Er3-O2 2.3561(6)	Er3-O3 2.3702(7)
Er3-O4 2.3572(6)	Er3-O4 2.3723(6)

Er3-O11 2.118(9)	Er3-O11 2.131(11)
Er3-O12 2.126(9)	Er3-O12 2.157(9)
Er3-O13 2.186(9)	Er3-O13 2.165(10)
Er4-O1 2.3799(6)	Er4-O2 2.3542(7)
Er4-O3 2.3602(6)	Er4-O3 2.3766(6)
Er4-O4 2.3631(6)	Er4-O4 2.3806(7)
Er4-O14 2.112(9)	Er4-O14 2.114(12)
Er4-O15 2.113(8)	Er4-O15 2.115(9)
Er4-O16 2.162(10)	Er4-O16 2.162(11)

Table S7. Selected bond angles (°) for ***R*-Er$_4$** and ***S*-Er$_4$**.

***R*-Er$_4$**	***S*-Er$_4$**
O2-Er1-O1 73.097(16)	O2-Er1-O1 73.54(2)
O3-Er1-O1 74.963(16)	O2-Er1-O3 74.19(2)
O3-Er1-O2 74.152(17)	O3-Er1-O1 73.85(2)
O5-Er1-O1 85.4(2)	O5-Er1-O1 85.9(3)
O5-Er1-O2 158.5(2)	O5-Er1-O2 95.2(3)
O5-Er1-O3 100.3(2)	O5-Er1-O3 159.0(3)
O5-Er1-O6 98.2(3)	O5-Er1-O7 100.6(4)
O5-Er1-O7 102.3(4)	O6-Er1-O1 161.9(3)
O6-Er1-O1 101.6(3)	O6-Er1-O2 89.0(3)
O6-Er1-O2 86.7(2)	O6-Er1-O3 97.0(4)
O6-Er1-O3 160.8(3)	O6-Er1-O5 100.9(4)
O6-Er1-O7 94.9(4)	O6-Er1-O7 94.6(4)
O7-Er1-O1 160.7(3)	O7-Er1-O1 100.7(3)
O7-Er1-O2 98.1(3)	O7-Er1-O2 162.8(3)
O7-Er1-O3 86.2(3)	O7-Er1-O3 88.6(3)
O2-Er2-O4 73.468(19)	O2-Er2-O1 73.184(18)
O3-Er2-O2 73.557(18)	O2-Er2-O4 74.741(18)
O3-Er2-O4 74.284(19)	O4-Er2-O1 73.445(17)
O8-Er2-O2 161.9(3)	O8-Er2-O1 87.2(3)
O8-Er2-O3 88.7(3)	O8-Er2-O2 160.4(3)
O8-Er2-O4 98.5(3)	O8-Er2-O4 101.7(3)
O8-Er2-O9 99.9(4)	O8-Er2-O10 95.0(5)
O8-Er2-O10 94.5(4)	O9-Er2-O1 159.1(3)
O9-Er2-O2 85.9(3)	O9-Er2-O2 100.8(3)
O9-Er2-O3 95.8(2)	O9-Er2-O4 85.7(3)
O9-Er2-O4 158.9(3)	O9-Er2-O8 98.1(4)
O9-Er2-O10 99.8(4)	O9-Er2-O10 101.3(4)
O10-Er2-O2 101.4(3)	O10-Er2-O1 98.4(3)
O10-Er2-O3 163.3(3)	O10-Er2-O2 86.4(3)
O10-Er2-O4 89.0(3)	O10-Er2-O4 160.9(3)
O2-Er3-O1 73.048(17)	O1-Er3-O3 73.35(2)
O2-Er3-O4 74.262(18)	O1-Er3-O4 73.297(18)

O4-Er3-O1 73.027(16)	O3-Er3-O4 73.292(18)
O11-Er3-O1 160.5(3)	O11-Er3-O1 98.9(3)
O11-Er3-O2 87.9(3)	O11-Er3-O3 163.0(3)
O11-Er3-O4 98.1(3)	O11-Er3-O4 90.1(3)
O11-Er3-O12 97.1(4)	O11-Er3-O12 97.1(4)
O11-Er3-O13 98.1(4)	O11-Er3-O13 97.6(4)
O12-Er3-O1 90.2(2)	O12-Er3-O1 86.9(3)
O12-Er3-O2 98.9(3)	O12-Er3-O3 97.6(3)
O12-Er3-O4 163.0(2)	O12-Er3-O4 159.8(3)
O12-Er3-O13 96.6(4)	O12-Er3-O13 98.2(4)
O13-Er3-O1 99.0(2)	O13-Er3-O1 162.0(3)
O13-Er3-O2 162.6(2)	O13-Er3-O3 88.8(3)
O13-Er3-O4 88.7(2)	O13-Er3-O4 99.5(3)
O3-Er4-O1 74.364(16)	O2-Er4-O3 73.349(19)
O3-Er4-O4 74.583(18)	O2-Er4-O4 74.229(18)
O4-Er4-O1 72.742(16)	O3-Er4-O4 73.030(18)
O14-Er4-O1 160.5(3)	O14-Er4-O2 99.1(4)
O14-Er4-O3 99.3(3)	O14-Er4-O3 87.9(3)
O14-Er4-O4 87.8(3)	O14-Er4-O4 160.8(3)
O14-Er4-O15 99.8(3)	O14-Er4-O15 99.6(4)
O14-Er4-O16 96.2(4)	O14-Er4-O16 96.2(5)
O15-Er4-O1 97.8(2)	O15-Er4-O2 83.9(3)
O15-Er4-O3 83.5(2)	O15-Er4-O3 157.0(3)
O15-Er4-O4 157.7(2)	O15-Er4-O4 97.5(3)
O15-Er4-O16 101.6(3)	O15-Er4-O16 101.7(4)
O16-Er4-O1 88.5(3)	O16-Er4-O2 162.6(3)
O16-Er4-O3 162.7(3)	O16-Er4-O3 99.0(3)
O16-Er4-O4 98.3(2)	O16-Er4-O4 88.6(3)

Table S8. The CShM values calculated by SHAPE 2.1 for ***R*-Er$_4$** and ***S*-Er$_4$**.[8, 9]

Central atom	Coordination Geometry	***R*-Er$_4$**	***S*-Er$_4$**
Er1	Octagon (D_{6h})	31.776	31.822
	Pentagonal pyramid (C_{5v})	25.728	24.496
	Octahedron (O_h)	1.376	1.731
	Trigonal prism (D_{3h})	11.458	10.280
	Johnson pentagonal pyramid J2 (C_{5v})	28.891	27.706

Central atom	Coordination Geometry	***R*-Er$_4$**	***S*-Er$_4$**
Er2	Octagon (D_{6h})	32.142	31.830
	Pentagonal pyramid (C_{5v})	26.151	26.054
	Octahedron (O_h)	1.321	1.323
	Trigonal prism (D_{3h})	11.618	11.969
	Johnson pentagonal pyramid J2 (C_{5v})	29.612	29.167

Central atom	Coordination Geometry	***R*-Er$_4$**	***S*-Er$_4$**
Er3	Octagon (D_{6h})	31.955	31.916
	Pentagonal pyramid (C_{5v})	24.330	25.431
	Octahedron (O_h)	1.716	1.502
	Trigonal prism (D_{3h})	10.388	11.187
	Johnson pentagonal pyramid J2 (C_{5v})	27.506	28.734

Central atom	Coordination Geometry	***R*-Er$_4$**	***S*-Er$_4$**
Er4	Octagon (D_{6h})	31.644	32.080
	Pentagonal pyramid (C_{5v})	25.464	26.291
	Octahedron (O_h)	1.461	1.354
	Trigonal prism (D_{3h})	11.214	11.540
	Johnson pentagonal pyramid J2 (C_{5v})	28.709	29.619

Table S9. Comparison of selected average Ln-OH and Ln···Ln distances (Å) of the cubane $[Ln_4(\mu_3\text{-}OH)_4]^{8+}$ (Ln = Dy, Er).

	***R*-Ln$_4$**/Å	***S*-Ln$_4$**/Å
Dy-OH	2.389	2.388
Dy···Dy	3.768	3.771
Er-OH	2.363	2.362
Er···Er	3.726	3.727

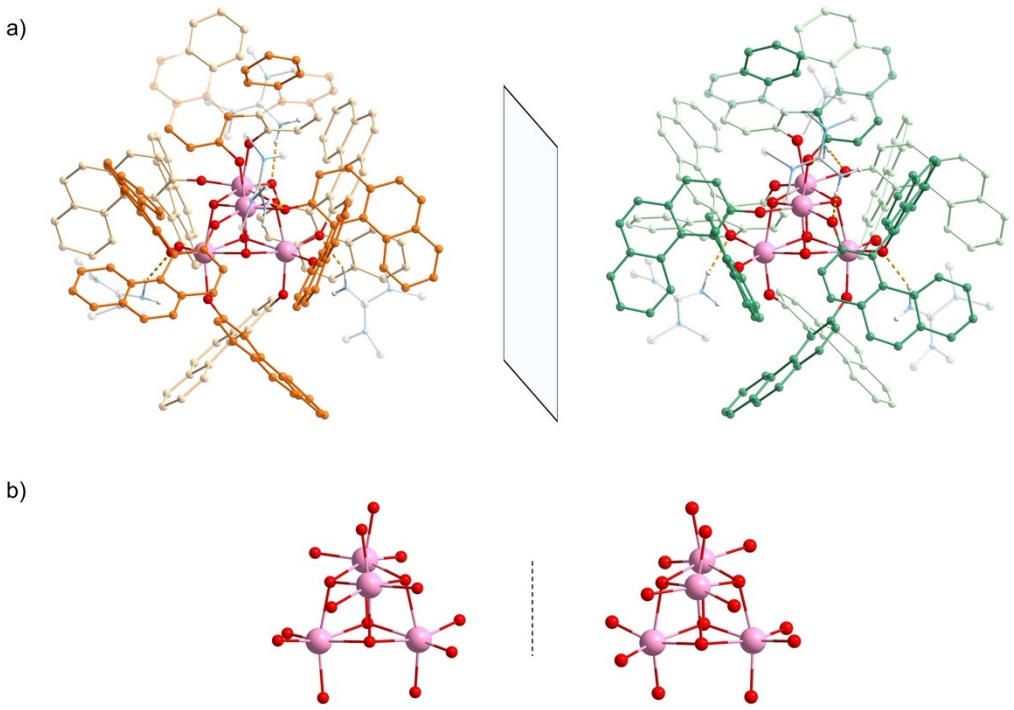

Figure S12. Molecular structures (a) and their corresponding cubane cores (b) of ***R*-Er$_4$** (right) and ***S*-Er$_4$** (left).

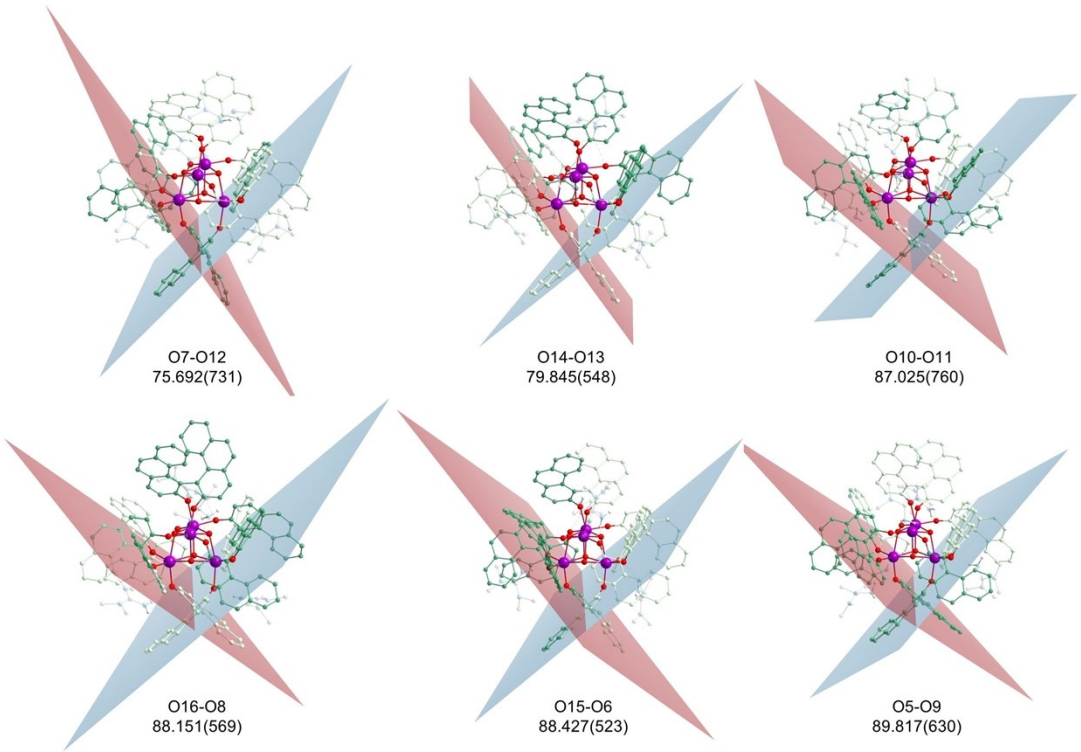

Figure S13. The dihedral angles of the six ligands in ***R*-Dy$_4$**.

Figure S14. The dihedral angles of the six ligands in ***S*-Dy$_4$**.

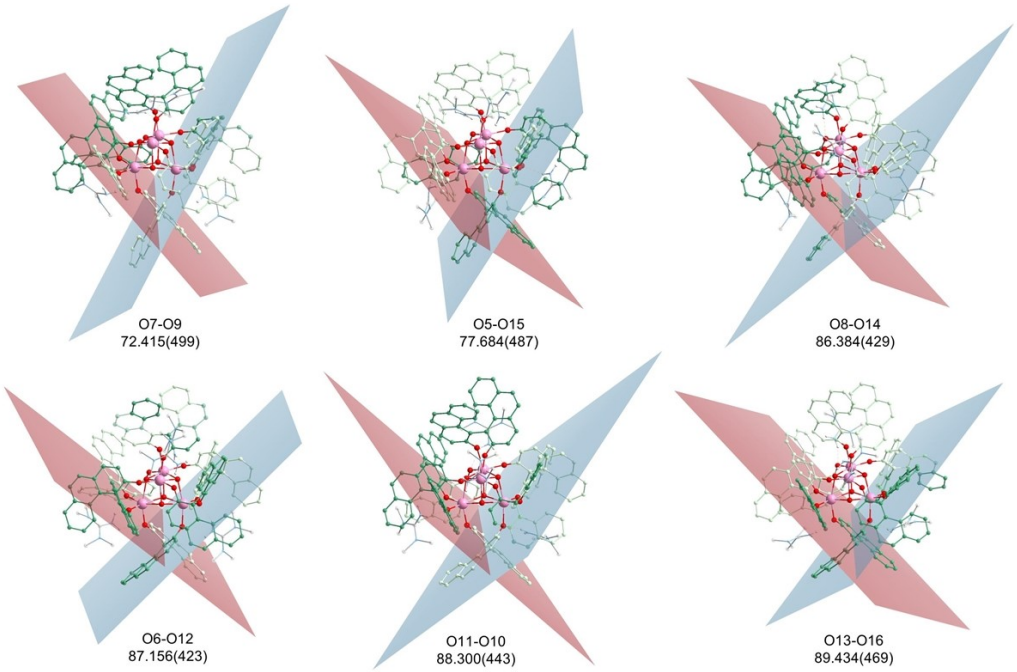

Figure S15. The dihedral angles of the six ligands in ***R*-Er$_4$**.

Figure S16. The dihedral angles of the six ligands in ***S*-Er$_4$**.

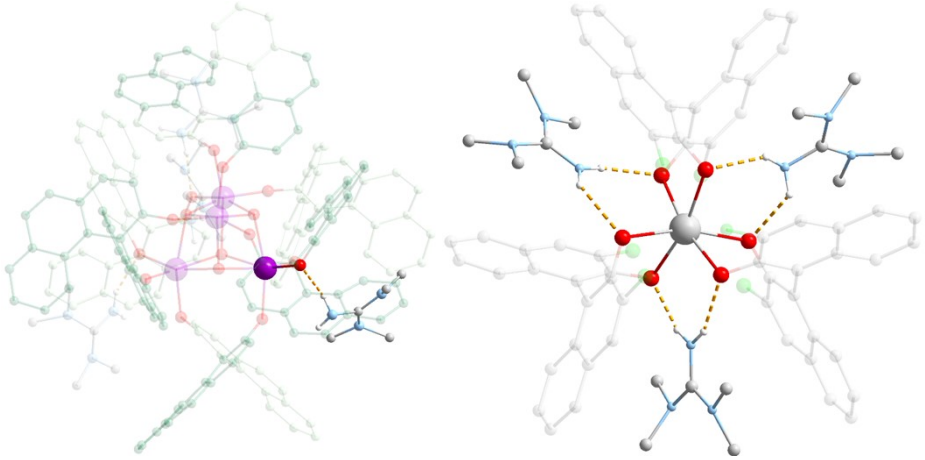

Figure S17. Molecular view highlighting the hydrogen-bonding (yellow dashed lines) interaction in ***R*-Dy$_4$** (left) and **(F$_2$Binol)$_3$Gd(TMG-H$^+$)$_3$** (right) with selected atoms shown in ball-and-stick representation: Dy (light purple), O (red), N (blue), C (light gray), and H (white).[10]

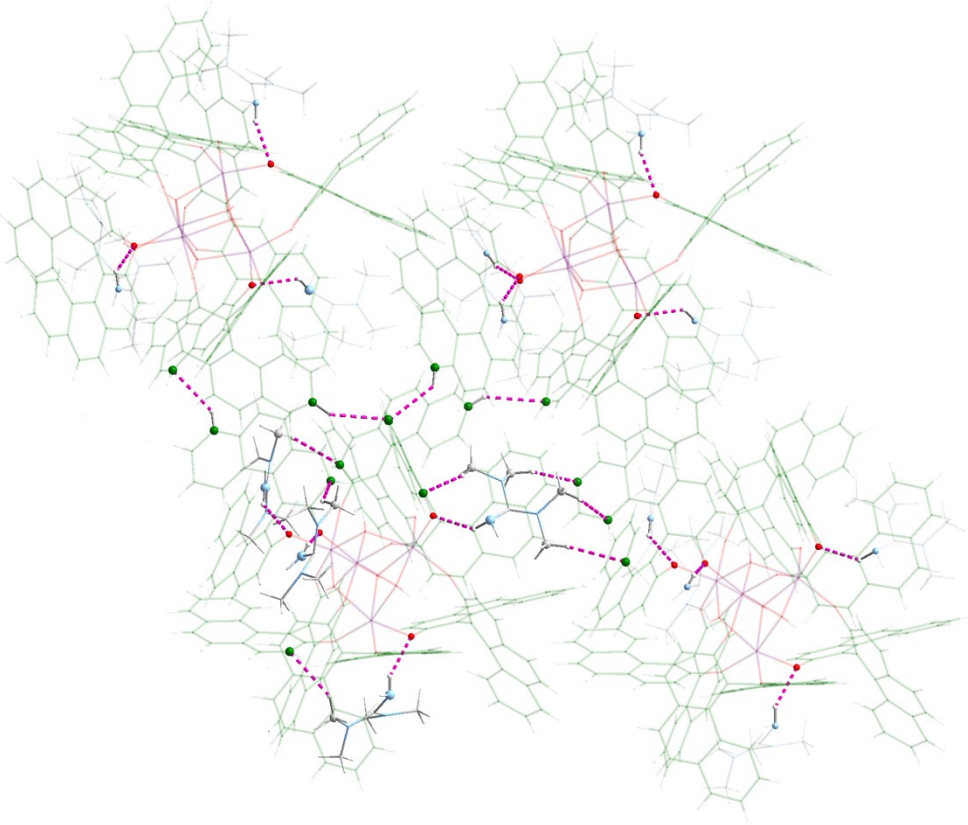

Figure S18. The packing diagram of ***R*-Dy$_4$** viewed along the crystallographic c axis, with intramolecular and intermolecular hydrogen bonds depicted as pink dashed lines. The carbon atoms of the guanidinium group are colored gray for clarity.

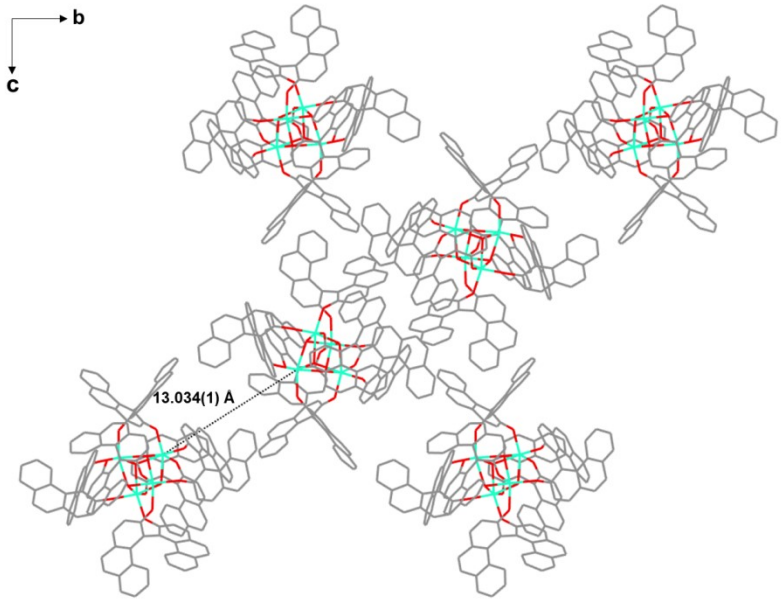

Figure S19. The packing diagram for ***R*-Dy$_4$** shown along the crystallographic *a* axis gives the shortest intermolecular Dy···Dy distance of 13.034(1) Å.

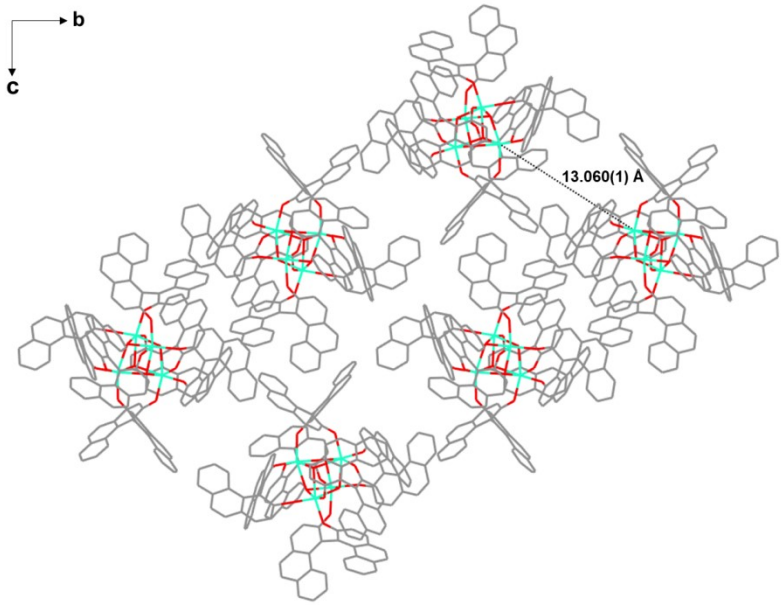

Figure S20. The packing diagram for ***S*-Dy$_4$** shown along the crystallographic *a* axis gives the shortest intermolecular Dy···Dy distance of 13.060(1) Å.

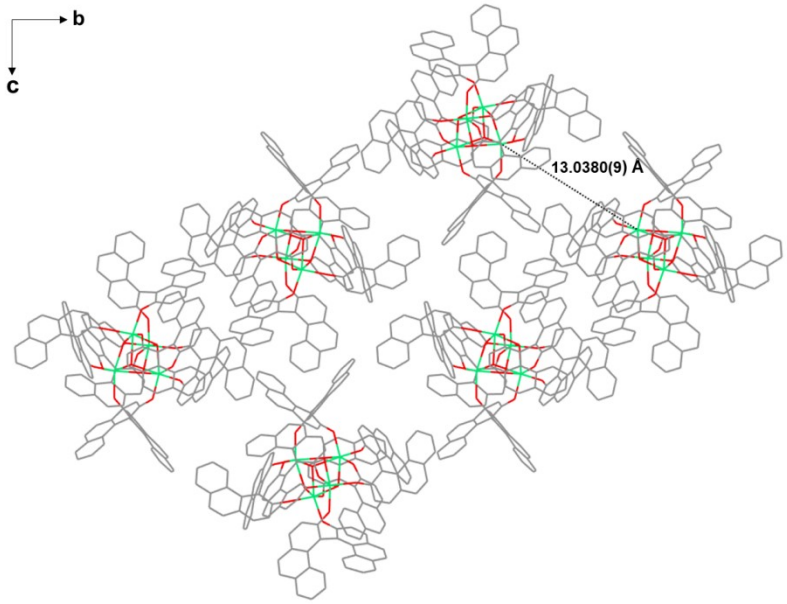

Figure S21. The packing diagram for ***R*-Er$_4$** shown along the crystallographic *a* axis gives the shortest intermolecular Er···Er distance of 13.0380(9) Å.

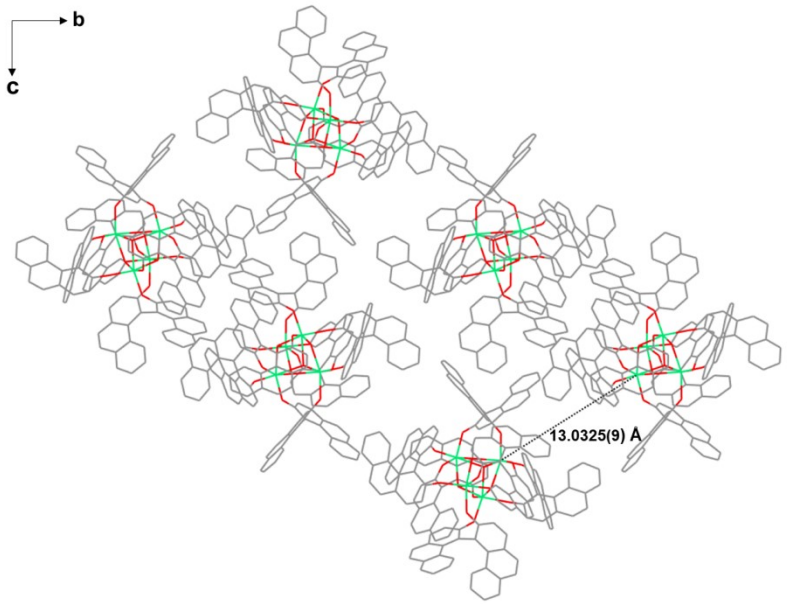

Figure S22. The packing diagram for ***S*-Er$_4$** shown along the crystallographic *a* axis gives the shortest intermolecular Er···Er distance of 13.0325(9) Å.

3. Magnetic measurements

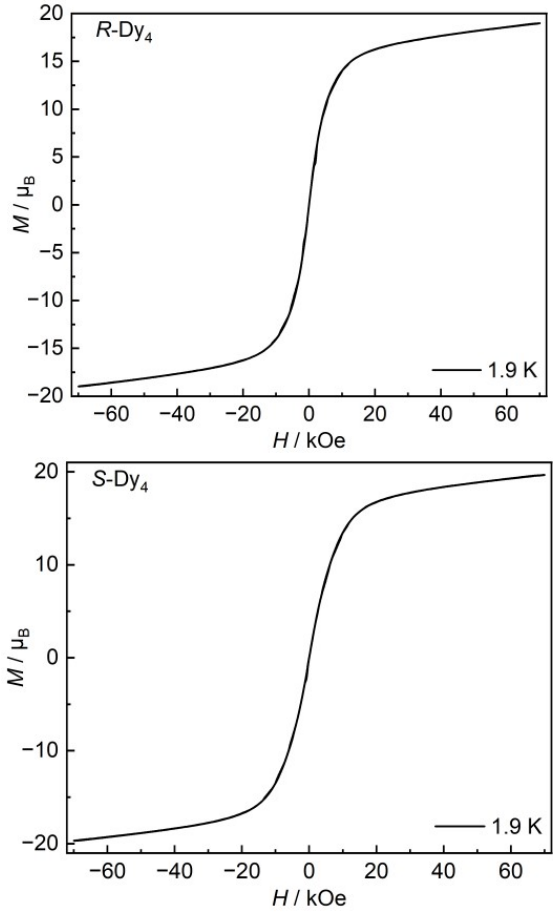

Figure S23. Magnetic hysteresis loops of ***R*-Dy$_4$** (top) and ***S*-Dy$_4$** (bottom) collected at 1.9 K.

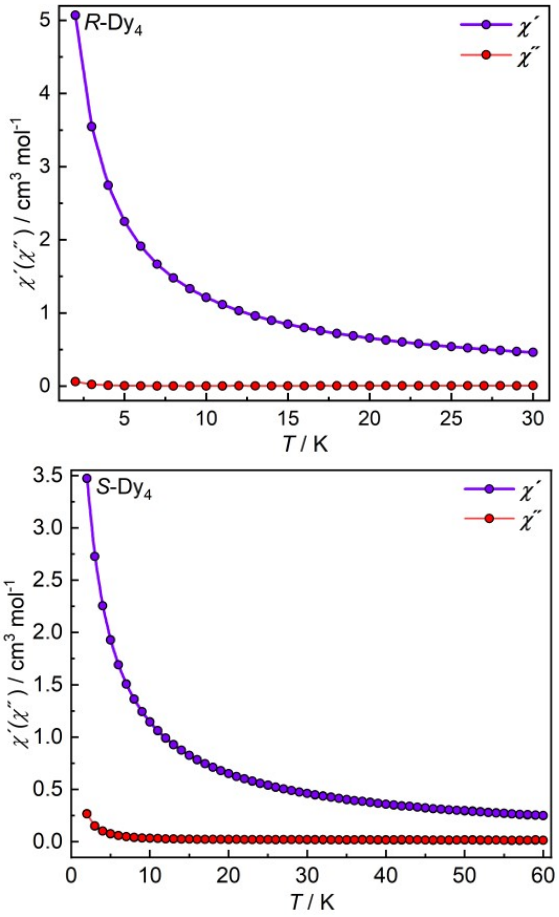

Figure S24. Temperature-dependent ac magnetic susceptibility of ***R*-Dy$_4$** (top) and ***S*-Dy$_4$** (bottom) under zero static dc field.

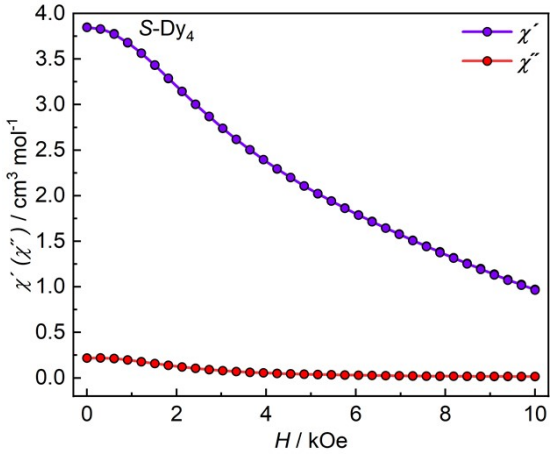

Figure S25. Field-dependent ac magnetic susceptibility of ***S*-Dy$_4$** at 1.9 K.

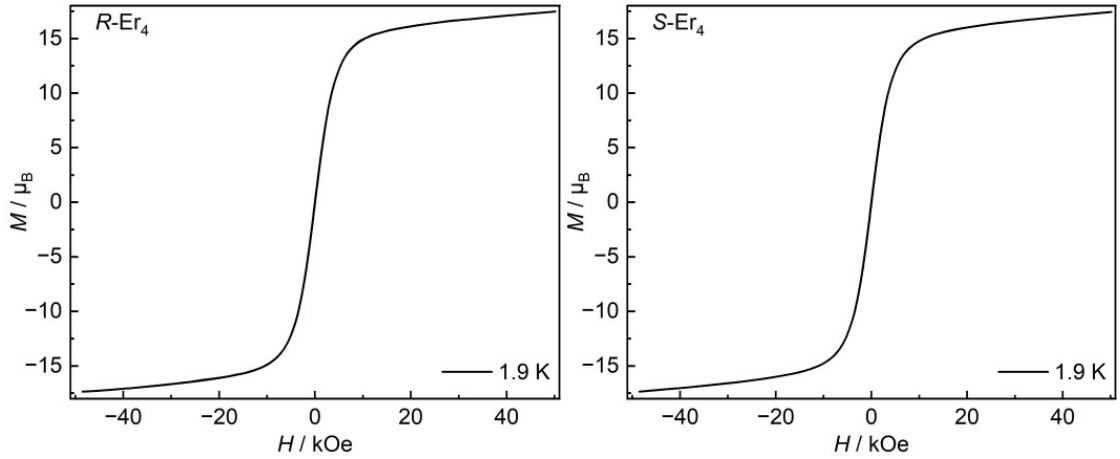

Figure S26. Magnetic hysteresis loops of ***R*-Er$_4$** (top), and ***S*-Er$_4$** (bottom) collected at 1.9 K.

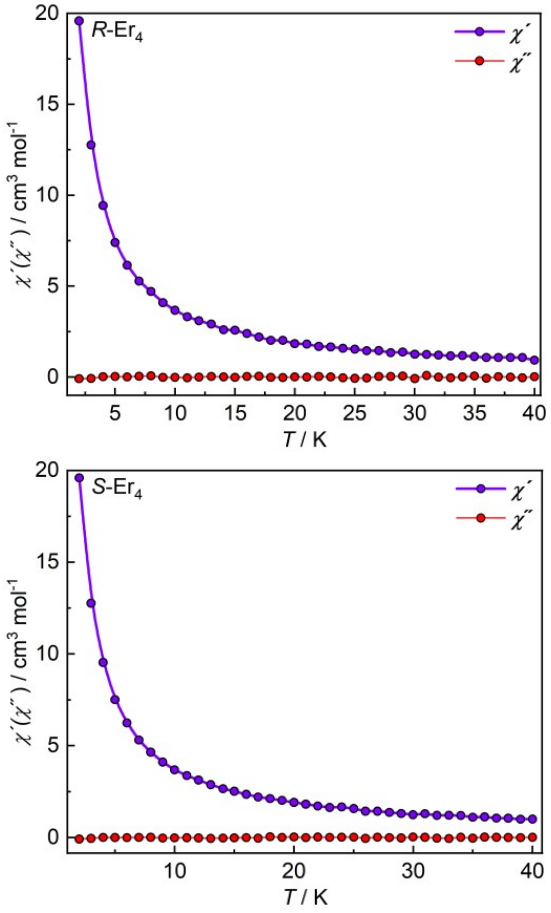

Figure S27. Temperature-dependent ac magnetic susceptibility of ***R*-Er$_4$** (top), and ***S*-Er$_4$** (bottom) under zero static dc field.

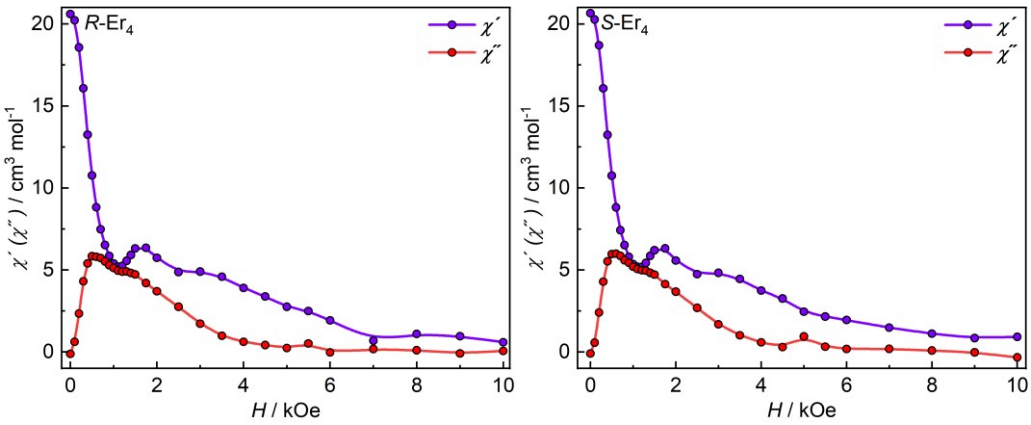

Figure S28. Field-dependent ac magnetic susceptibility of ***R*-Er$_4$** (left), and ***S*-Er$_4$** (right) at 1.9 K.

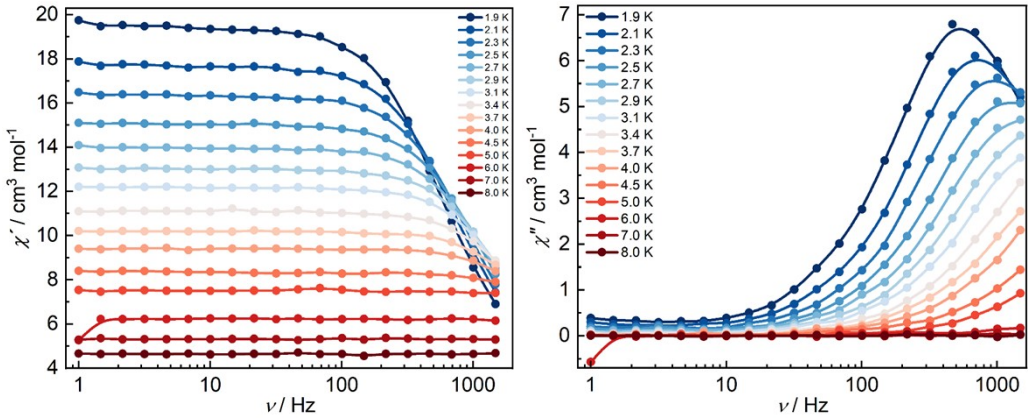

Figure S29. Temperature dependence of the AC susceptibility χ' (left) and χ'' (right) data for ***S*-Er$_4$** under a 600 Oe applied field.

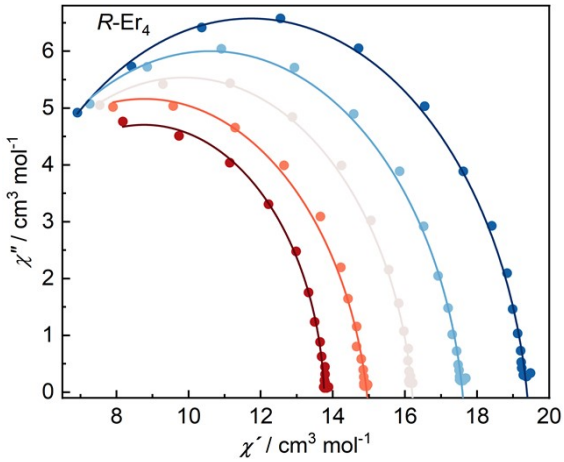

Figure S30. Cole-Cole plots for ***R*-Er$_4$**. The solid lines are obtained by fitting experimental data to the generalized Debye model.

Table S10. The relaxation fitting parameters for ***R*-Er$_4$** from fitting ac data at varying temperatures.

T (K)	χ_S	χ_T	τ	α
1.9	1.08E+00	5.01E+00	2.92E-04	9.11E-02
2.1	9.90E-01	4.54E+00	2.22E-04	8.50E-02
2.3	9.85E-01	4.18E+00	1.82E-04	7.12E-02
2.5	8.88E-01	3.85E+00	1.43E-04	7.33E-02
2.7	8.47E-01	3.57E+00	1.19E-04	6.82E-02

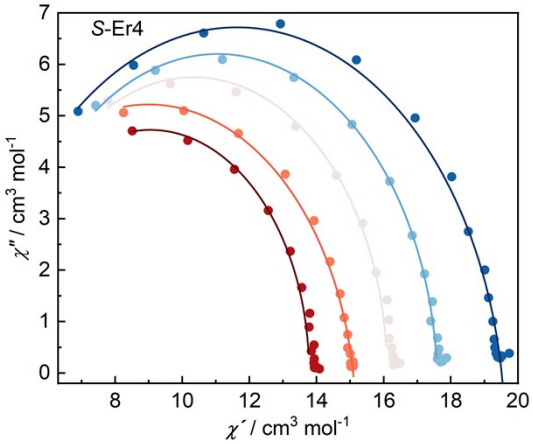

Figure S31. Cole-Cole plots for ***S*-Er$_4$**. The solid lines are obtained by fitting experimental data to generalized Debye model.

Table S11. The relaxation fitting parameters for ***S*-Er$_4$** from fitting ac data at varying temperatures.

T (K)	χ_S	χ_T	τ	α
1.9	1.61E+00	7.55E+00	2.79E-04	7.80E-02
2.1	1.58E+00	6.86E+00	2.15E-04	6.68E-02
2.3	1.47E+00	6.34E+00	1.70E-04	6.27E-02
2.5	1.43E+00	5.83E+00	1.37E-04	6.13E-02
2.7	1.44E+00	5.42E+00	1.17E-04	5.35E-02

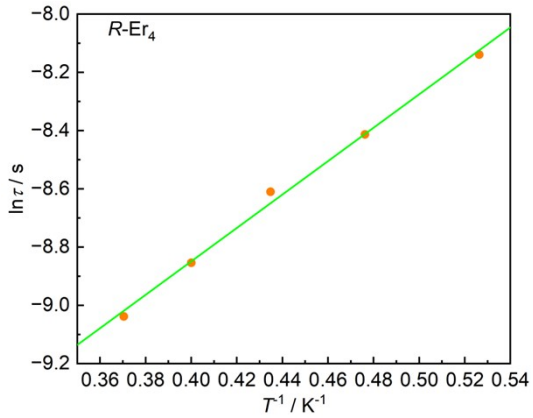

Figure S32. Temperature dependence of the relaxation time in the form of natural logarithm for ***R*-Er$_4$**. The green line represents the fitting. Inset: The temperature when Orbach have the same relaxation rate was determined by the second derivative of the plot log(τ^{-1}) vs. log(T). The fitting equation is ln(τ) = - ln[τ_0^{-1}exp(-U_{eff}/k_BT)], giving U_{eff}/k_B = 5.74(22) K, $\tau_0 = 10^{-4.84(4)}$ s.

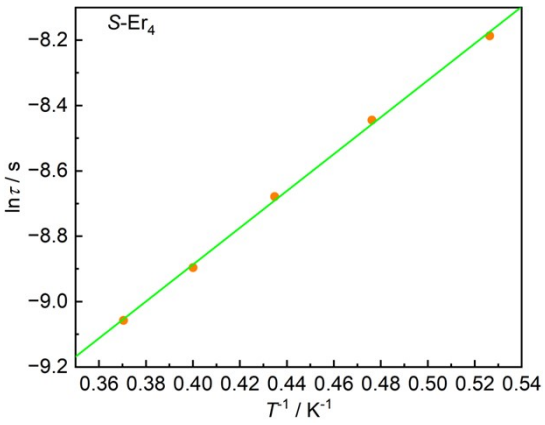

Figure S33. Temperature dependence of the relaxation time in the form of natural logarithm for ***S*-Er$_4$**. The green line represents the fitting. Inset: The temperature when Orbach have the same relaxation rate was determined by the second derivative of the plot log(τ^{-1}) vs. log(T). The fitting equation is ln(τ) = - ln[τ_0^{-1}exp(-U_{eff}/k_BT)], giving U_{eff}/k_B = 5.64(11) K, $\tau_0 = 10^{-4.84(2)}$ s.

Table S12. Single-Molecule Magnet Properties of Ln_4 Complexes

Compound[a]	U_{eff} (K)[b]
[$Er_4(\mu_3$-OH)$_4$(*R*-L)$_6$(TMG-H$^+$)$_4$] (*this work*)	5.74
[$Er_4(\mu_3$-OH)$_4$(*S*-L)$_6$(TMG-H$^+$)$_4$] (*this work*)	5.64
[$Dy_4(\mu_3$-OH)$_4(\mu$-tfa)$_4$(hfa)$_4$(phen)$_4$][11]	67.0
[Dy_4(L)$_4(\mu_2$-$\eta_1\eta_1$Piv)$_4$]·4H_2O·6CH_3OH[12]	43.4
[$Dy_4(\mu_3$-OH)$_4$(L)$_4(\mu_2$-piv)$_4$(MeOH)$_4$][13]	26(500 Oe)
[$Dy_4(\mu_3$-OH)$_2(\mu_3$-O)$_2$(cpt)$_6$(MeOH)$_6$(H_2O)]$_2$[14]	—
[$Dy_4(\mu_3$-OH)$_4$(isonicotinate)$_6$(py)-(CH_3OH)$_7$]·(ClO_4)$_2$·py·4CH_3OH[15]	—
Dy_8(HL)$_{10}$($C_6H_4NH_2COO$)$_2(\mu_3$-OH)$_8$(OH)$_2$(NO_3)$_2$(H_2O)$_4$[16]	—
[$Dy_4(\mu_3$-OH)$_4$(Acc)$_6$(H_2O)$_7$(ClO_4)]·(ClO_4)$_7$·11H_2O[17]	—
[$Dy_4(\mu_3$-OH)$_3(\mu_3$-O)(NOPyCOO)$_6$(OH)(H_2O)$_3$·(DMF)$_3$(H_2O)$_{12}$]$_\infty$[18]	—

[a] Compound displays any out-of-phase ac susceptibility signal. [b] — indicate no peak maxima can be found in the out-of-phase ac susceptibility plot.

4. References

1. T. Matsushima, S. Kobayashi and S. Watanabe, *J. Org. Chem.*, 2016, **81**, 7799-7806.
2. M. Jakubec, T. Beránek, P. Jakubík, J. Sýkora, J. Žádný, V. Církva and J. Storch, *J. Org. Chem.*, 2018, **83**, 3607-3616.
3. A. K. Swain, K. Radacki, H. Braunschweig and P. Ravat, *J. Org. Chem.*, 2022, **87**, 993-1000.
4. E. A. M. Boudreaux, L. N., *Theory and Applications of Molecular Paramagnetism*, John Wiley & Sons, New York, 1976.
5. O. V. Dolomanov, L. J. Bourhis, R. J. Gildea, J. A. K. Howard and H. Puschmann, *J. Appl. Crystallogr*, 2009, **42**, 339-341.
6. G. Sheldrick, *Acta Cryst. C*, 2015, **71**, 3-8.
7. G. Sheldrick, *Acta Cryst. A*, 2015, **71**, 3-8.
8. D. Casanova, J. Cirera, M. Llunell, P. Alemany, D. Avnir and S. Alvarez, *J. Am. Chem. Soc.*, 2004, **126**, 1755-1763.
9. M. Pinsky and D. Avnir, *Inorg. Chem.*, 1998, **37**, 5575-5582.
10. T. Feng, R. Cai, Z. Zhu, Q. Zhou, A. Sickinger, O. Maury, Y. Guyot, A. Bensalah-Ledoux, S. Guy, B. Baguenard, B. Le Guennic and J. Tang, *Chem. Eur. J.*, 2025, **31**, e202500910.
11. H.-Y. Wong, W. T. K. Chan and G.-L. Law, *Inorg. Chem.*, 2018, **57**, 6893-6902.
12. S. Das, A. Dey, S. Biswas, E. Colacio and V. Chandrasekhar, *Inorg. Chem.*, 2014, **53**, 3417-3426.
13. A. Rasamsetty, C. Das, E. C. Sañudo, M. Shanmugam and V. Baskar, *Dalton Trans.*, 2018, **47**, 1726-1738.
14. D. Savard, P.-H. Lin, T. J. Burchell, I. Korobkov, W. Wernsdorfer, R. Clérac and M. Murugesu, *Inorg. Chem.*, 2009, **48**, 11748-11754.
15. Y. Gao, G.-F. Xu, L. Zhao, J. Tang and Z. Liu, *Inorg. Chem.*, 2009, **48**, 11495-11497.
16. H. Ke, P. Gamez, L. Zhao, G.-F. Xu, S. Xue and J. Tang, *Inorg. Chem.*, 2010, **49**, 7549-7557.
17. J.-B. Peng, Y.-P. Ren, X.-J. Kong, L.-S. Long, R.-B. Huang and L.-S. Zheng, *CrystEngComm*, 2011, **13**, 2084-2090.
18. X. Yi, K. Bernot, G. Calvez, C. Daiguebonne and O. Guillou, *Eur. J. Inorg. Chem.*, 2013, **2013**, 5879-5885.